2020

Assessing 3D Printability of Bioinks

Nicole Ramirez
University of Central Florida

ASSESSING 3D PRINTABILIY OF BIOINKS

by

NICOLE RAMIREZ

A thesis submitted in partial fulfillment of the requirements
for the Honors in the Major Program in Mechanical Engineering
in the College of Engineering and Computer Science
and in the Burnett Honors College
at the University of Central Florida
Orlando, Florida

Spring Term 2020

Committee:

Dr. Dazhong Wu (Chair)

Dr. Melanie Coathup

Abstract

The field of tissue engineering (TE) is continuously improving through the use of additive manufacturing techniques (AM) such as three-dimensional (3D) bioprinting. The 3D bioprinter has significantly gained attention in the TE field because it is more efficient than regenerative medicine and is readily available as opposed to organ transplants. Working like a conventional 3D printer, the 3D bioprinter is able to dispense material layer by layer from the bottom up with the printing head able to move in the X, Y, and Z direction. This movement allows for the fabrication of structures with complex geometries. In this study, the shape fidelity of additively manufactured specimens was explored in order to define consistent results for extrusion-based bioprinting techniques. Parallel to the importance of this emerging technology, the development of bioinks also demands for active research. While many bioink research efforts line up with the development and creation of printable inks for extrusion-based bioprinting, bioink printability is largely ignored and still needs to be carefully examined to enable improvement in fabrication. This thesis describes a reproducible method for the assessment of the printability of bioinks, focusing first on the creation of the bioink followed by the analysis of the 3D printed structures. Material selection is a critical component of efficient 3D bioprinting because of the requirements needing to be fulfilled to adhere to suitable bioink formulation. To address the importance of bioprinting, inspecting deformations of the deposited filament, reviewing its printability and evaluating the printing parameters will contribute to the assessment of shape fidelity. By characterizing the combination of material and printing parameters, it is hypothesized that this approach may evolve into a true assessment of bioprintability.

Table of Contents

List of Figures

List of Tables

List of Acronyms

AM: Additive Manufacturing

CAD: Computer-Aided Design

ECM: extracellular matrix

ESC: Embryonic Stem Cell

FDM: Fused Deposition Modeling

PBS: Phosphate-buffered saline

STL: stereolithography

TE: Tissue Engineering

UV: Ultraviolet Light

1. Introduction

Biofabrication is a relatively young field of research believed to improve the field of tissue engineering (TE) through the implementation of additively manufactured (AM) technologies. With the advancement of this technology, it was suggested many years ago that 3D printing of tissues and organs should cater to the needs of patients who are on the organ donation waiting list [1]. 3D bioprinting is significant in contributing to these desired biofabrication applications because it provides a platform to make different bioinks [2]. The research being conducted in this area target the enduring and unsolved challenges in TE and regenerative medicine. A challenge faced in this interdisciplinary field that limits the development of biofabrication techniques involve material selection not only for its availability, but also the compatibility to create a suitable bioink. It is recognized that the bioink must be printable when tuning the biological properties and associated mechanical properties. Printability is defined by the rheological properties of the materials and must be adjusted to the fabrication process used to generate constructs with high shape fidelity [3]. Printability for a bioink is defined by the fluidity of the printer features during print and the structures resemblance to the initial input after print completion. A structure that demonstrates ease of printing and displays high quality resolution by maintaining its structure, is distinguished with having good printability. There are three different types of bioprinting methods that researchers have tried in order to improve the printability of bioinks [4].

The three different bioprinting strategies exploited to print structures of complex geometries are inkjet [5], laser-assisted [6] and extrusion-based [7]. Due to the increasing complexity needed for tissue fabrication, 3D bioprinting is facing several challenges in all the

production processes. The list of requirements for a suitable bioink have outlined challenges, and these include printability, biocompatibility and necessary structural/mechanical properties [8]. Inkjet bioprinting functions very similarly to the classic 2D inkjet printing. A low viscosity bioink is loaded into a cartridge that is connected to a printhead with a piezoelectric or heating element. Through the piezoelectric vibrations, the bioink is forced out as droplets from the printhead nozzles [9]. This method enables contactless printing and offers a variety of other advantages along with some disadvantages. In laser-assisted bioprinting, printers use lasers focused on an absorbing substrate to generate pressures that transfer biomaterials onto a substrate by propelling the bioink forward. Lastly, the extrusion-based bioprinting method is a 3D printer equipped with pneumatic driven pistons, that continuously dispense filament and deposits layers that adhere together to create a 3D structure. This method is commonly used and in fact, this contact-based printing technique is typically considered to be inferior to the other two in regard to resolution. Printing resolution is affected by its relationship with cell viability: the higher the nozzle gauge, the higher the printer resolution [9]. Although there a three bioprinting processes that have been used to fabricate 2D/3D constructs, limitations and challenges remain. Through comparison of the three current bioprinting techniques in *Table 1***,** it can be inferred that the extrusion-based printing technique is generally considered to be the most popular primarily because of its commercial availability amongst other factors. For a visual that illustrates the functionalities of the three bioprinting techniques, see *Figure 1* below. The three bioprinting methods fall under the branch of AM technologies, whose functional capabilities are the basis of consecutive addition of layers of material to create 3D structures.

Table 1: Pros and Cons of Current Bioprinting Techniques

Current Bioprinting Techniques		
Inkjet	ADVANTAGES	• Low cost • High printing speeds • Contactless printing that avoids contamination
	DISADVANTAGES	• Bioink viscosity is commonly limited to < 15 MPa • The settling effect of biological cells that may occur in the bioink reservoir [11, 12] can obstruct the nozzle and cause heterogeneity of printed structures • The droplets in inkjet printing are typically in the pico-litre (pl) scale resulting in rapid drying that can occur post-ejection [35] which has proven detrimental to cell survival after deposition [13]
	ADVANTAGES	• It is a non-contact printing technique; thus, clogging of the bioink and living matter is avoided • The technique allows a wide range of bioink viscosity (1–300 MPa) resulting in printing without significantly affecting cell viability or function • It is possible to work with high cell densities up to 108 cells/mL. [14–16]

Laser	DISADVANTAGES	• Printing multiple cell types requires time-consuming preparation of individual cell-laden layers [17,18] • Generation of cell-laden droplets is random due to the spreading nature of the cell-laden layer, which requires using a near-confluent cell-laden layer [19] • The cost can be relatively higher than other printing techniques
Micro-extrusion	ADVANTAGES	• Very similar to conventional fused deposition modeling (FDM) 3D printing • Commercially available • It has the ability to extrude bioinks of high-cell density [20] • Extrusion printing enables the operator to create heterogeneous models by depositing different types of cells at initial controlled locations and cell number within a pre-designed structure. [10] • Relatively affordable, and the instrumentation can be highly customizable with respect to the desired structure or bioink

	DISADVANTAGES	• Mammalian cell viability is often lower than found in models created using inkjet-based bioprinting (40%–85%), primarily due to the resultant shear stress that occurs at high extrusion pressures. [21–23] • Printing resolution and speed

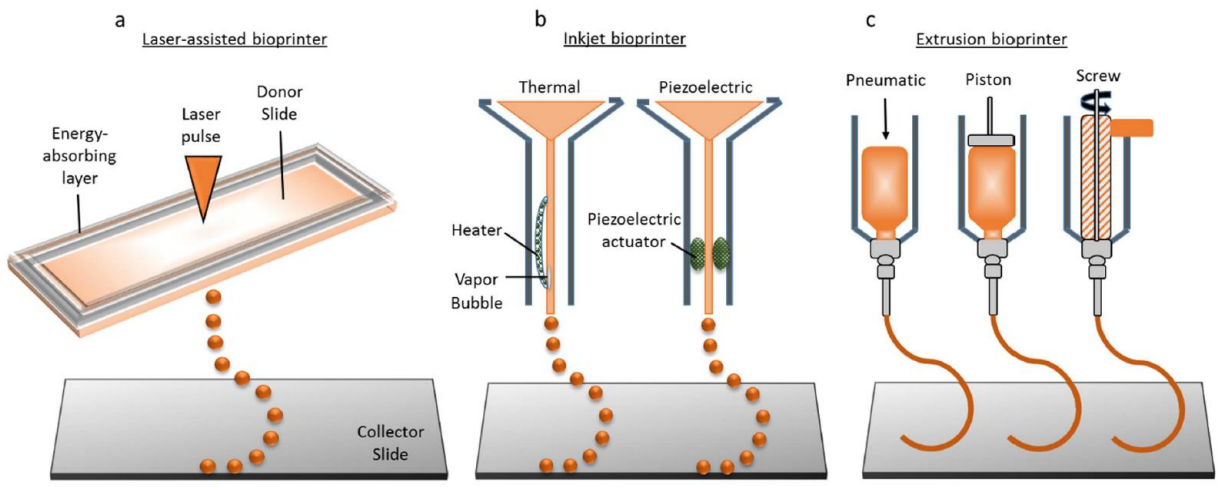

Figure 1: Three current bioprinting techniques [24]

Although, there are reports that discuss the formulation of many bioinks, significant research on the assessment of 3D printed bioinks needs to be conducted with the goal of improving printability. This thesis focuses on the importance of bioink printability for bioprinting implementation. Bioink is a material used to encapsulate cells to provide a supportive extracellular matrix (ECM) environment and safeguard cells from the stresses a cell has to undergo during printing. The bioink printability is generally characterized by the controllable formation of the

deposited filament and shape fidelity of each extruded layer [9]. The objective of this thesis is to assess the printability of extrusion-based bioprinting to participate in the improvement of shape fidelity. The correlation between printing parameters and bioink consistency contribute to the printability performance. Printing parameters that play an important role in achieving a good resolution construct include the dispensing pressure, printing speed, nozzle diameter, nozzle temperature and printbed temperature [25]. In order to define the printing parameters, the properties of the bioink also need to be considered. For this experiment, several bioink concentrations were created with different portions of GelMA® and alginate. GelMA® is a material composed of gelatin; a hydrolyzed collagen obtained from various sources like pork or calf skin and fishes, [26] and a photo-initiator. The purpose of a photo-initiator is to facilitate cross-linking within the ink allowing it to retain its shape post processing. Several methods are used to crosslink bioinks, including Ultra-Violet (UV) light, ionic cross-linking, and temperature change. The purpose crosslinking serves is to preserve the structures shape fidelity. Alginate is a naturally occurring polysaccharide and is a commonly employed material in bioinks [26]. Different bioinks respond differently to the variation of printing parameters, thus parameters that need to be carefully considered with respect to these two materials are temperature and dispensing pressure as they adjust the viscous properties of the bioink in preparation for print.

Similar to a conventional 3D printing procedure, an STL file of the digital model desired for print needs to be created using computer-aided design (CAD) [27, 28]. Once the 3D CAD model is complete, it is then transferred to the 3D bioprinter that processes the file into layers to communicate a layer by layer extrusion along 3-axis. The complex geometric structures from the CAD file make it challenging to precisely extrude the desired AM part. To address this issue,

printing properties such as pressure, temperature, nozzle size, and velocity are manipulated to reduce discrepancies and ensure a precise print. In this Honors in the Major thesis, the assessment of the printability of a GelMA® and alginate bioink of varying concentrations were investigated under a set of predefined printing parameters.

2. Literature Review

2.1. Printability of Hydrogels

Correlated to material selection, hydrogels have also been widely used in 3D bioprinting to store cells for TE. Closely resembling the objective of this thesis, He, Y. et al. [29] performed a series of experiments that investigated the printability of hydrogels of varying printing parameters, because this topic is seldom addressed. The methodology of the experiments performed transition from 1D (printed lines) to 3D structures while observing printing accuracy. Success in printability was dependent on the structure accuracy. Printing failures were considered along the Z direction as observable filament collapse and the fusion of adjacent layers. Success was demonstrated through the harmonization of printing parameters with a 3D printed hydrogel scaffold.

Hydrogels are accepted as a biomaterial with attributed biocompatibility, which is why they are used as the cell-laden materials for bioprinting. Using the extrusion-based bioprinting method to precisely control the deposition of cell-laden hydrogels, organs may be mimicked better as the 3D structures determine the growth characteristics of cells after printing. In the research of hydrogel printability, much focus has been on the assessment of the printability of the ink solutions, in order to find a direct correlation between printability and the hydrogel mechanical properties [30]. However, few researchers have drawn their attention to the relationship between printing parameters and printing fidelity. This mentioned study focused on expanding research reports for discussing the printability of biomaterials or the relationship between printability and printing parameters.

2.2. Effect of Bioink Properties on Printability

To reiterate, there is a research gap for characterizing the influences of printing parameters on shape fidelity of 3D constructs as well as on cell viability after the printing process. To contribute to this research gap, a study was carried out that systematically analyzed the influence of bioink properties and printing parameters on bioink printability and embryonic stem cell (ESC) viability in the process of extrusion-based cell printing, also known as bioplotting [31]. This demonstrates another study that once again shares a similar research objective of assessing the printability of bioinks, however the assessment of cell viability was omitted in this thesis although it is a future concern for the important features discussed in this referred to study.

The adopted method of this study was to first evaluate the rheological properties of gelatin and alginate to better understand the corresponding bioink features under different bioink compositions and printing parameters. Printability was then characterized to properly assess the structure through the accepted viability ranges and the defined printing parameters. To achieve a successful 3D cell printing procedure, this study acknowledges that the influence of bioink properties and printing parameters on either bioink printability or cell viability need to both be accounted for to achieve the desired results. This thesis aims to provide criteria and tools to begin the evaluation of printing parameters and bioink characteristics for an alginate/gelatin composition for use in extrusion-based bioprinting. The temperature sensitivity of gelatin to print multilayered construct and the rapid ionic crosslinking of alginate for long-term culture [32, 33] are amongst the important takeaways that influence printability.

2.3. Using Rheological Parameters to Assess Bioink Printability

Gao et al. [34] performed a study that sought to develop a framework for evaluating printability. Analogous to the bioink concentration in this thesis, gelatin and alginate were the hydrogels used to develop various concentrations. Upon the formulation of these hydrogels, they were evaluated to quantitatively define values for the ideal printing parameters. Factors such as extrudability, extrusion uniformity, and structural integrity were given attention for determining good printability results. The methodology in this example could be used to evaluate the printability of the bioinks created for this paper. Successful results from the study include gelatin-alginate composite hydrogels that exhibited an excellent compromise between structural integrity and extrusion uniformity.

Hydrogels are typically unable to be self-supportive upon layer-by-layer deposition, which is why it is usually required to be cross-linked directly after printing [34-37]. The intention is to prevent collapsing or sagging after printing and maintaining a high shape fidelity during the printing process when fabricating multi-layered porous structures [38]. An alternative approach presented in this study to address the limitations of hydrogel availability, include the utilization of supporting and sacrificial materials. However, this approach imposes other restrictions because of the addition of new biological properties associated with the support material. Therefore, it was touted to define printing parameters for a printable bioink material. Smoothness extrudability remained within this definition as displaying good printability and was measured manually in ImageJ software where the uniformity of each filament was analyzed. This experiment prompted the use of ImageJ to analyze the extruded structure.

3. Methodology

As previously stated, the research objective was to test varying concentrations of GelMA® and alginate extruded-based bioink concentrations to assess their printability. Initial tests were performed where temperature and speed were altered and the effect on shape fidelity and printability in 3D bioprinting determined. To fulfill this study objective, the following steps were taken: (1) to create an in-house bioink, (2) to compile CAD files for the structures prior to print and, (3) to collect corresponding experimental data while testing the variability in printing parameters for the printable alginate-gelatin bioink developed.

The materials used when creating the in-house bioink consisted of two hydrogels: gelatin (GelMA powder) and alginate. Hydrogels have a low viscosity and consequently are prone to filament collapse, damaging the entire structure [39]. The mixture for the solution occupies lab distinguished properties, so the aim was to reach ideal bioink properties to enable smooth extrusion. Moreover, to improve printability the bioink properties such as viscosity needed to be adjusted to agree with the combination of alginate and gelatin. Therefore, temperature and material selection are crucial elements that effect the bioink consistency and assist in determining if it is printable. It became apparent through initial experimentation that creating a bioink that can withstand the viscosity threshold, is critical because the ink properties change instantaneously during the printing process due to an immediate temperature change.

Finally, step three in the study objective was to make sense of the preliminary data that was collected through the tests performed. Drawing conclusions to make progress towards defining appropriate printing parameters in the manipulation of additively manufactured mechanical

properties like printing speed, printhead temperature and printing pressure. Documenting the process taken to its entirety so that this experiment can be replicated or further carried out to the fullest extent was an addition aim, striving towards the goal of biofabricated 3D printed organs. Data was analyzed using IBM SPSS Statistics 25 software using a Mann-Whitney test where P=0.05 were considered significant changes in printability. It is also implied that the methodology reported in this thesis explains the detailed experimental process and the course of action taken throughout the year of research.

4. Materials and Method

4.1. Bioprinting System – CELLINK BIO X

CELLINK BIO X (Celllink® Life Sciences, USA) is the printer used to perform experiments in the Additive Manufacturing and Intelligent Systems Laboratory at the University of Central Florida (Figure 2). It is user-friendly and offers features like:

- Heated printheads.
- Cooled printheads.
- Heated print bed.
- Cooled print bed.
- Clean Chamber Technology.
- Piston-driven syringe head.
- Pneumatic printheads.
- Multi well-plate printing.
- Touchscreen control.

Figure 2: BIO X 3D Bio Printer

This standalone system also gives users flexibility with exchangeable printheads.

The structural design of this machine is optimized externally and internally. With a machine size of 480x440x355 mm (H/W/D), these fitting dimensions spare open spacing because of its compact tabletop standard. Some of the internal specifications include a power input of 100-230 V, 50-60 Hz, 400 W and this system conveniently supports STL and G-code file types. All CAD models tested in the proceeding experiments were saved as STL file types to allow for data transfer

to the computer system. An illustration of the bioprinting process for this extrusion-based bioprinter is shown below (Figure 3) to demonstrate the motion of the printhead moving along the X and Y plane with print speed directed towards the left and the pneumatic operation along the Z axis to extrude the hydrogel contained within the nozzle.

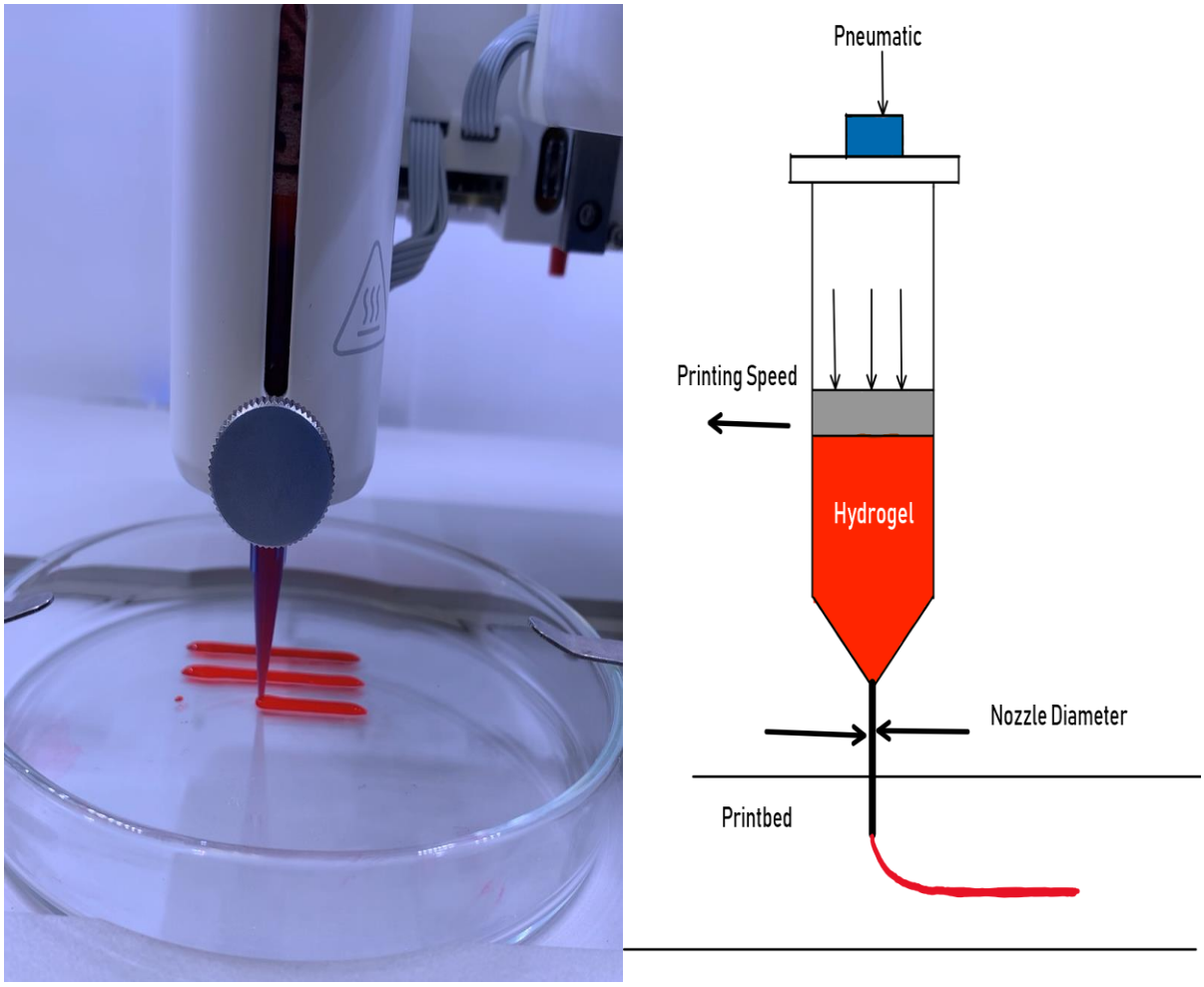

Figure 3: Applied extrusion-based 3D bioprinting

4.2. Bioink Preparation

Various approaches have been taken by previous researchers in the development of bioink concentrations, however, techniques to assess their shape fidelity after bioprinting have been

neglected and could potentially benefit the study of printability [40]. The subsequent experiments address the progressing creation of the original in lab made bioink that consists of different concentrations made of 6% alginate, which remains constant and is mixed with gelatin that ranges from 2-6%.

For this particular study, the steps taken for bioink preparation have been simplified to reduce the time and effort taken to create multiple bioink concentrations. Taking into consideration that alginate remains constant at 6% within each concentration, the experiment calls for a desired total of 20 mL of phosphate-buffered saline (PBS), to be filled in a graduated cylinder. As gelatin is introduced to the mixture, this desired total prevents the addition of alginate all the while keeping it constant at 6%. The calculation for alginate added is as follows:

$$20\ mL * 0.06 = 1.2\ g\ alginate$$

A scale was used to weigh 1.2 grams of alginate. The measured total of 20 mL PBS was achieved using a pipette for accuracy to then transfer the water-based salt solution into a graduated cylinder. Additionally, the 1.2 grams of alginate was poured into the cylinder and a stirring-magnet was gently placed into the cylinder to mix the solutions. Securely clamped onto the stirring scale, the exposed portion of the graduated cylinder was then covered with aluminum foil to avoid evaporation. Once all the items were properly contained, the stirrer was then slowly turned on to reach a rotation speed of about 800 rpm and was done so to visibly observe movement in the magnet. The location of the graduated cylinder needed to be adjusted so that the rotating magnet is aligned at its center, this is necessary to optimize the functionality of the mixer so it successfully dissolves the added material (Figure 4). After the location was calibrated the next step was to

increase magnetation and the speed of the stirrer by turning the knob clockwise. No heat was applied. For optimal results, the experiment was left stirring overnight to ensure the total decomposition of the alginate powder.

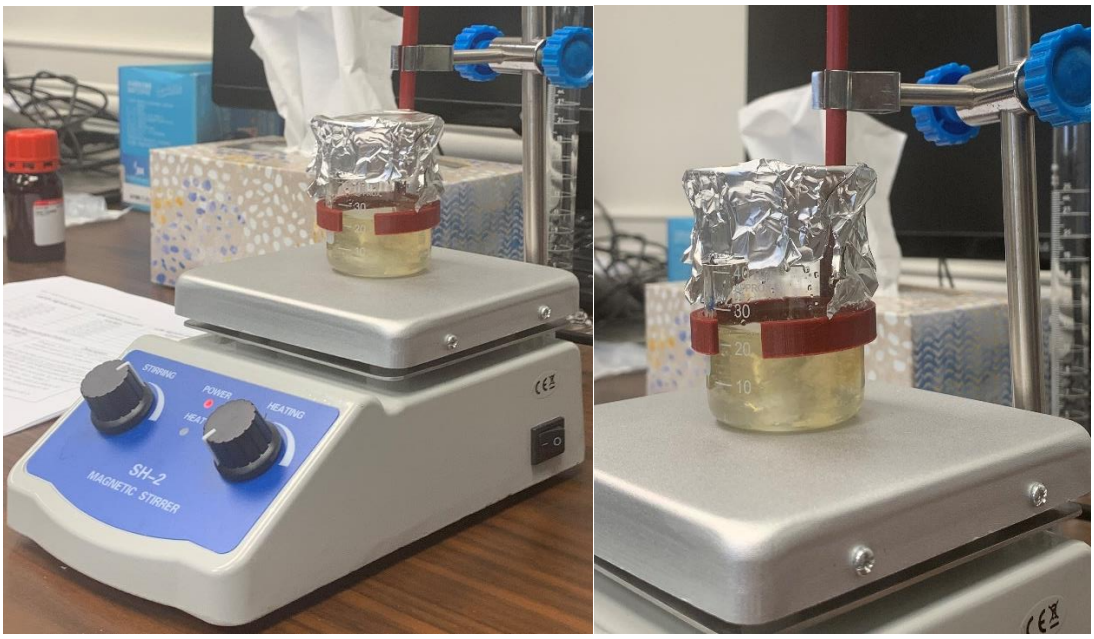

Figure 4:Alginate bioink concentration on SH-2 Magnetic stirrer

Upon returning to check for an observable change and verifying the powder was fully dissolved, the next step for preparation was to add the desired amount of GelMA® powder. The beaker remained on the platform, but the stirrer was turned off once the powder was confirmed to have dissolved. Three different bioink concentrations were created and investigated in this Honors in the Major thesis. A heat source is required to initiate conduction in order to completely dissolve the GelMA powder. Turning the knob clockwise (will be located next to the stirrer knob) to operate the heat, increasing it to reach a temperature reading of 70 degrees Celsius. Before preceding to add the GelMA powder, a few drops (0.1%) of a dark red food coloring solution (New Coccine from Sigma Aldrich) were added to improve visualization of the filaments and assist data

collection and analysis. As a transparent ink proved difficult to view following printing, the red dye enhanced the clarity of the bioink and its edges allowing for more accurate analysis. In this study, 0.1% (0.02 g) of dye was added. Analogous to the alginate powder, gelatin was weighed on the scale and then transferred to the graduated cylinder for each of the concentrations. Table 2 below displays the different concentration compositions investigated for each recorded measure of gelatin powder. Each concentration is held in a 3 mL syringe which was deducted from the desired total. Therefore, the amount of gelatin powder was calculated based on the total amount remaining in the cylinder after each syringe deduction.

Table 2: Bioink Gelatin Composition

Parameter	**Concentration Values**		
Gelatin (%)	2	4	6
Gelatin Powder (g)	0.34	0.28	0.22

The calculation used to determine the amount of gelatin powder was:

$$Total\ gelatin\ powder = (Cylinder\ total - 3\ mL) * (0.02)$$

The cylinder total begins at the desired total of 20 mL and was subtracted by 3 mL for each time a syringe was filled. The gelatin range increases by an increment of 2 which is why it was multiplied by 2% to obtain the total amount of gelatin powder to be added for each concentration. Table 3 below comes directly from the manufacturers of the 3D bioprinter (Cellink® Life Sciences, US) and served as a reference for the bioink preparation process.

Table 3: Suggested concentration from Cellink [41]

GelMA-Alginate Bioink	wt% GelMA precursor solution	wt% Alginate precursor solution
5%-1.5%	10% GelMA	3%
7.5%-1.5%	15% GelMA	3%
10%-1.5%	20% GelMA	3%
5%-3%	10% GelMA	6%
7.5%-3%	15% GelMA	6%
10%-3%	20% GelMA	6%

4.3. Experimental Setup

The field of tissue engineering is still at its early stages in research and thus prompts different paths to be taken depending on the desired research direction. Despite there being different focuses on 3D bioprinting, the unanimous goal is to develop functional 3D printed organs. Many researchers have reviewed the formulation of bioinks, but this thesis addresses the lack of attention given to the printability of the basic structure in 3D bioprinting. The structure reviewed and used in this study is shown in Figure 5 and was evaluated as having good printability if the extruded structure accurately printed it at the pre-determined dimensions of 30 mm (length) and 0.2 mm (width). Having the same dimensions, three lines on the same CAD file were printed to document any extruded discontinuities within the same test by comparing the three rods parallel to each other. This CAD model was selected as the basis for assessing printability because it corresponds to smooth extrudability if the line avoids discontinuities within the structure. Discontinuities may be caused by poor bioink properties such as a highly viscous bioink that is impeded on extrusion by clogging the nozzle. The model diameter of the rod was modified to be less than the nozzle tip diameter explicitly to avert nozzle clogs and is therefore a solid trajectory line of the printhead.

For this reason, other factors such as the biomaterial properties were attributed with causing discontinuities, resulting in poor printability.

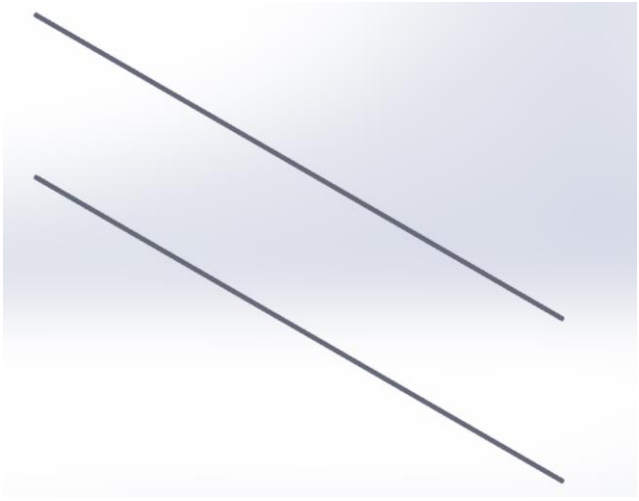

Figure 5: 3D CAD Structure

Advancing to the experimental set up, it is not at all complex because it follows a 3D printing process. Part of the experimental set up was to have an already prepared bioink concentration at hand as established in the previous section.

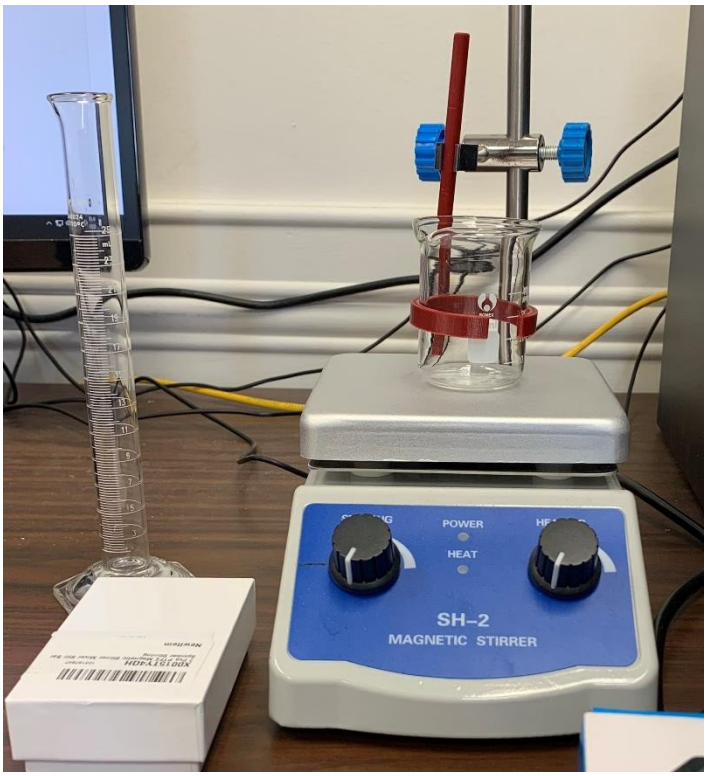

Figure 6: Experimental set up for bioink preparation

The materials needed in order to conduct the experiment include the prepared bioink concentration, 0.22-gauge nozzles, wipes, a circular glass plate, and cotton swabs. Gloves were also utilized as a safety precaution. The need for multiple nozzles was also a precautionary measure for the instances where there was a clogged nozzle that needed to be replaced.

Having the required materials, the next step toward conducting the experiment was to change the viscosity of the bioink concentration to adapt to room temperature so that it may extrude smoothly. Placing the syringe in the first printhead of the BIO X printer and adjusting the settings to read 32 degrees Celsius for the first pneumatic tool will heat the printhead containing the bioink.

This took approximately 15- 20 minutes to reach the required temperature. Alginate is the consistence substance in the bioink, so it was considered to be stable for moderate temperature change. During the heating processes, the printbed temperature was also adjusted in the settings menu to reach 12 degrees Celsius so that once the bioink was extruded, this optimal temperature hardens the deposited bioink, resulting in a retention in shape fidelity. After the target temperatures were reached, the syringe was then removed from the printhead and a 0.22-gauge nozzle attached. Returned to its initial printhead, the cap at the top of the syringe was also removed and the pneumatic pressure tool attached. Table 4 presents the parameters kept constant prior to and during printing. The other settings were to be adjusted according to the ink being tested. This experiment alternated in the shift of speed and pressure for each temperature that changed in intervals of 10 degrees Celsius. The first printing parameter that was tested for each bioink was pressure which incrementally changed by an order of 5 kPa with printing speed held constant at the default speed of 20 mm/s to target concise results by analyzing one printing parameter at a time. The main parameters for the first test subject of these different tests are summarized in Table 5 and closely resembles a combination of **Error! Reference source not found.** and *Table 3* because it refers to the bioink formulation. This concludes the settings adjustment in the experimental setup.

Table 4: Constant parameters in the printer settings

CONSTANT PARAMETERS		
Pneumatic Temperature (°C)	Printbed Temperature (°C)	Nozzle Size (gauge)
32	12	22

Table 5: Main parameters for different tests

Test Index	1-1	1-2	1-3	1-4	1-5	2-1	2-2	2-3	2-4	2-5	3-1	3-2	3-3	3-4	3-5
Bioink	2% Gel + 6% Alg					4% Gel + 6% Alg					6% Gel + 6% Alg				
Pressure (kPa)	20	25	30	35	40	20	25	30	35	40	20	25	30	35	40

Moving forward, a trial was carried out both to test for functional extrusion and fill of the nozzle tip with bioink. The nozzle tip was filled with bioink prior to running tests because it could negatively influence the results by delaying the deposit time for the filament because the print distance was already taken into account from the nozzle tip and not at its end. A wipe was placed on the printbed to contain the extruded bioink trial and the rain drop icon was then selected on the printer screen (held down for the amount extruded) to initiate extrusion. The extrusion appeared to be smooth which confirmed that the experiment was ready to be performed. For any remaining residue of bioink left on the nozzle tip, the cotton swab was used to carefully remove the bioink while avoiding damage to any equipment.

4.4. Rheological Properties

With a focus on printability, it is important to also investigate the impact of the rheological properties of each bioink. Understanding the rheological or mechanical properties of gelatin plays a critical role in the biomedical industry. When a gelatin solution is cooled below the sol–gel transition temperature, the coil molecules form triple-chain helices through renaturation of collagen-like spirals, and the solution transforms into a three-dimensional gel structure [42], providing strength and elasticity. Due to the immense differences in gelatin and alginate, the properties of the two hydrogels change when mixed together because the temperature criteria for strengthening these two materials has to satisfy the new bioink consistency. In relation to the

manipulation of printing properties in this study, Bulcke et al. [43] used rheological measurements to characterize the mechanical properties of the chemically formed networks. He found that the cross-linked gelatin led to highly controllable chemical networks, suggesting that the final gel properties can be controlled through the degree of substitution or the storage conditions. Paxton et al. [43] outlined a method to assess printability requiring rheological measurements because of its usefulness to gain information about ink properties important for printing. The table below was sought to assist in the development of the mixed hydrogel concentration for this thesis which prompts for the comparison of rheological properties because the same materials were used. Although this groups study acted as the foundation for assessing printability, several factors such as percentage bioink concentration as well as the optimal temperature associated with the rheological properties were adjusted to remain within the constraints of ideal printability.

Table 6: Viscosity (ln η) of the mixture of sodium alginate and gelatin (37 °C, Concentration, %w/v) [29].

	C/Soduim alginate				
C/gelatin	1%	2%	2.5%	3%	4%
2%	4.93	7.10	7.81	8.45	9.51
4%	5.37	7.59	8.42	8.68	9.74
6%	6.08	7.82	8.57	8.98	10.11
8%	6.50	8.12	8.85	9.39	10.43
10%	6.72	8.68	9.19	9.69	10.60

4.5. Measuring printability in bioinks

Printability of the extruded product is represented by the ratio of printed line width and nozzle tip diameter which was measured and accounted for using ImageJ software. Focus was drawn on the variability in line width of the three lines printed to verify the best suitable parameters for

printing by analyzing the accuracy of the print to the provided CAD model. Printability was tested through the consideration of the effect speed, pressure, and nozzle tip diameter had on the extruded bioink concentration.

ImageJ is a public domain Java image processing and analysis program that can calculate area and pixel value statistics of user-defined selections. It can also automatically measure distances and angles through a gray scale calibration, which proved to be useful in that it saved time in performing manual calculations. Once the image was manually captured, ImageJ can then generate density histograms and line profile plots to concisely sum up the data collected. An imbedded feature in the software includes exporting the compiled data into an excel sheet that will clearly display values such as length, area, and average line width. Using those values to display a trend line that explores the change in line width over time as different factors such as speed and pressure were adjusted contributes to the assessment of good printability by analyzing the processed results. An example of the results collected from ImageJ may be found in Appendix A and just below it, the corresponding exported excel tables may be found in Appendix B.

Although, ImageJ was the resource utilized in this experimental data collection, there are some limitations associated with the software. The first step for automatically processing the captured microscopic image of the printed line is to set a scale for the properties to be measured. In this experiment, a 5 mm scale was used and remains consistent for the daily experiment performed. However, the scale length is prone to error because it does not remain the same for data collected on different days. A sacrifice is also made when processing the image because it also considers noise in the image. Even though, the threshold can be adjusted before confirming the selected area, it still over detects scatter in the image or under detects parts of the image, consequently hindering

the accuracy of the data. Despite these challenges, ImageJ was still considered the best method to document data.

5. Experimental Results

After the successful fabrication of various bioink concentrations as well as the several experiments performed, findings need to be analyzed and further interpreted in order to draw conclusions. Comparing successful and failed results from each experimental trial assists in defining printing parameters by interpreting the factors that caused the experiment to fail or otherwise achieve smooth extrudability. Until now, documental data of the initial experiment have been omitted because all tests failed. The very first bioink created was made solely of GelMA and as seen in **Error! Reference source not found.**, demonstrated shear thinning which prevented the containment of the bioink because of its poor viscous properties. It was then considered that the addition of another hydrogel component could prove to be advantageous to enhance its strength and allow for the assessment of printability to occur. Referred to several times in this thesis as being commonly used in bioprinting; alginate is the hydrogel that was mixed with GelMA to create new bioink concentrations.

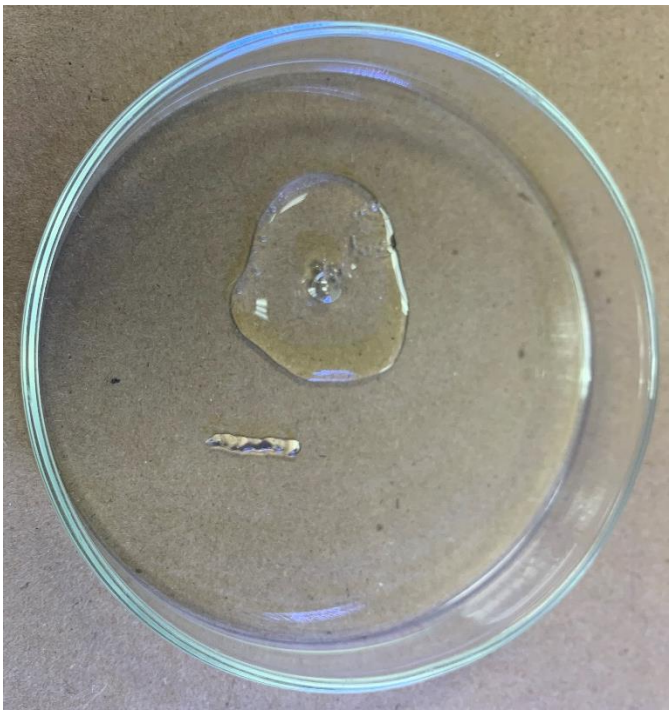

Figure 7: Failed experimental test

The second set of bioink concentrations created consisted of 2% alginate, which was held constant within 2, 4 and 6% gelatin. The same process for bioink preparation as discussed in the Experimental Setup section was followed by evaluating the same printing parameters as seen in Table 5. However, with the intent of running five tests on the first two concentrations (10 tests total), it was apparent that 2% alginate provided low viscous properties at the desired temperature reading. Adjusting the temperature would mean adding another variable parameter to be monitored, which would confuse the data. The two parameters to be changed throughout the experimental process were speed and pressure, yet neither had an effect on this bioink concentration because of how attenuated its consistency was. It was also noted that the nozzle would clog immediately after a print, preventing further experiments to be conducted without changing the nozzle prior to each trial run, however it could not exceed the trial run because it

would clog after the extrusion test. This test was recognized as having failed due to the bioink properties having credited alginate as the main contributor because the temperature threshold was not met to be able to change the viscous properties in preparation for extrusion. The two failed tests previously stated are contributors to the iterative process in developing new bioink concentrations that exhibit extrudable properties. Once the new and printable bioink concentrations were developed, discontinuity in the extruded print was used to the printability of bioinks.

A structure that demonstrates ease of printing and displays high quality resolution by maintaining its structure, is distinguished with having good printability. Past experiments resolved the issues faced with the consistency of the bioink concentration. Having confirmed that the new concentrations are in fact printable, the printing parameters were adjusted to fine tune any discrepancies within the print to achieve accurate printability. An example of poor printability may be observed in Figure 8 because it fragments the extrusion and is unidentifiable to the initial CAD model. The solution to print continuously and near accuracy (attributes of good printability) was found by tuning two printing parameters, pressure and speed.

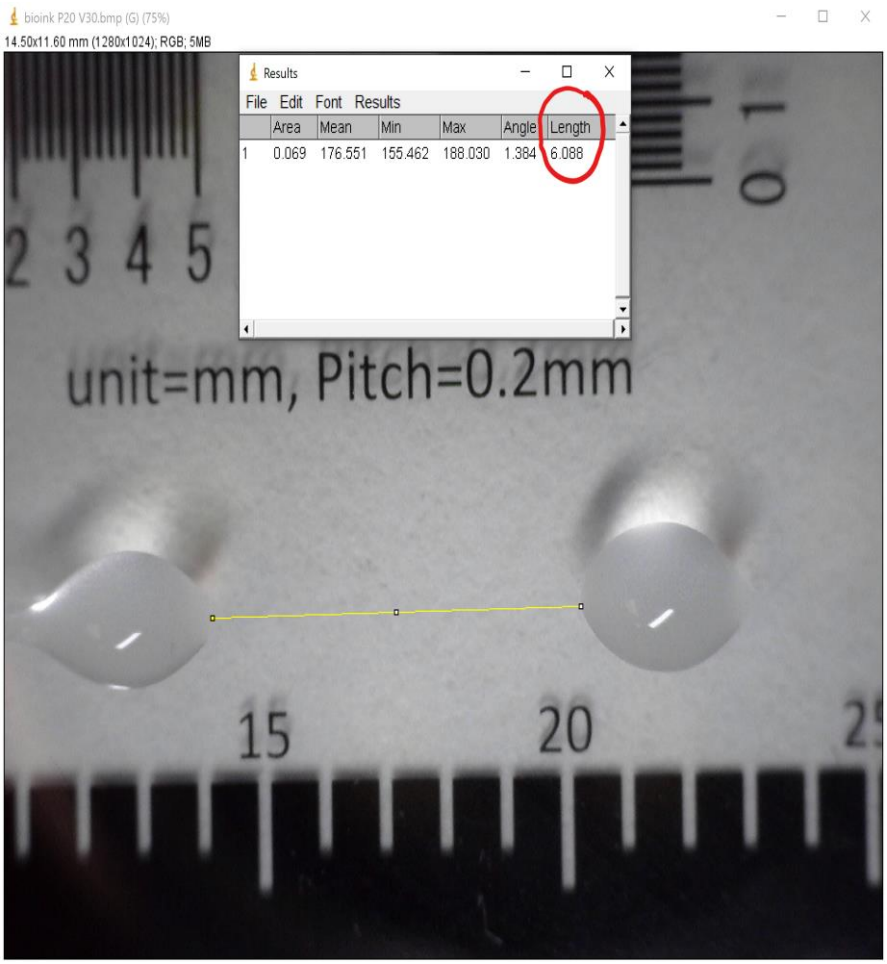

Figure 8: Calculated length discontinuities

The proceeding experiments were successful once the alginate percentage was corrected to 6%. Appendix B: Excel Results, outlines the area that was automatically captured in ImageJ along with the mean, max and min of the threshold captured. It is observed in the tables in descending order that the area increases when pressure increased, and speed remained constant. Comparing the images below, keeping speed constant at 20 mm/s and changing the pressure for a series of five tests allowed for the depiction of the best result by analyzing the printed line width and documenting the test that was close to the diameter of the CAD model. It was observed that the best result in terms of printing accuracy occurred at the lowest pressure (Figure 9) and is claimed

so because it resembles the accuracy of the CAD model and showcased ease of extrusion. The worst result was taken at the highest pressure of 40 kPa (Figure 10) because it exceeded the line length of the CAD model making this an inaccurate print.

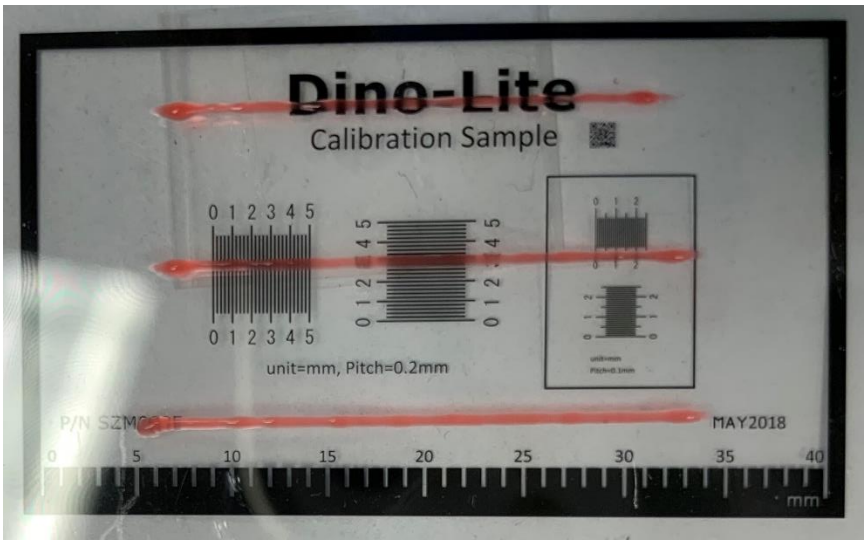

Figure 9: Pressure 20 kPa at a speed of 20 mm/s

Figure 10: Pressure 40 kPa at a speed of 20 mm/s

Figure 11: Pressure 40 kPa at a speed of 10 mm/s

Further analyzing the worst result in an attempt to improve its printability from the experiment where the speed was held constant, the associated pressure of 40 kPa was then held constant and speed was the parameter to be changed for a series of five experiments. This was done to test the correlation speed and pressure have to each other when assessing the printability of a smooth extruded bioink. The figure above is prudent because at a higher pressure and a lower speed, the printer should be able to precisely dispense extruded material. To verify this statement, *Figure 12* shows the trendline for average line width for an increase in pressure and an increase in speed. The data for the trendline is exported from ImageJ and shown in Table 7 and Table 8 where 'P' and 'S' correspond to pressure and speed values respectively, which pertains to the attributed values of the printed line. The standard error is also given for each measured line to statistically assess printability by analyzing significant differences in the interpreted data. For example, changes in printability according to speed in terms of accurate line width, found that the thickest line width was printed at a pressure of 20 kPa and a speed of 10 mm/s, with a mean of 1.508 +/-

0.016 kPa, resulting in poor printability. Changes in printability according to pressure provided the most accurate results by displaying the thinnest line width was produced from having a pressure of 20 kPa and a speed of 20 mm/s with a mean of 0.845 +/- 0.006 kPa, indicating a significant difference (P=0.05) but with good printability because of its near accuracy to the CAD model.

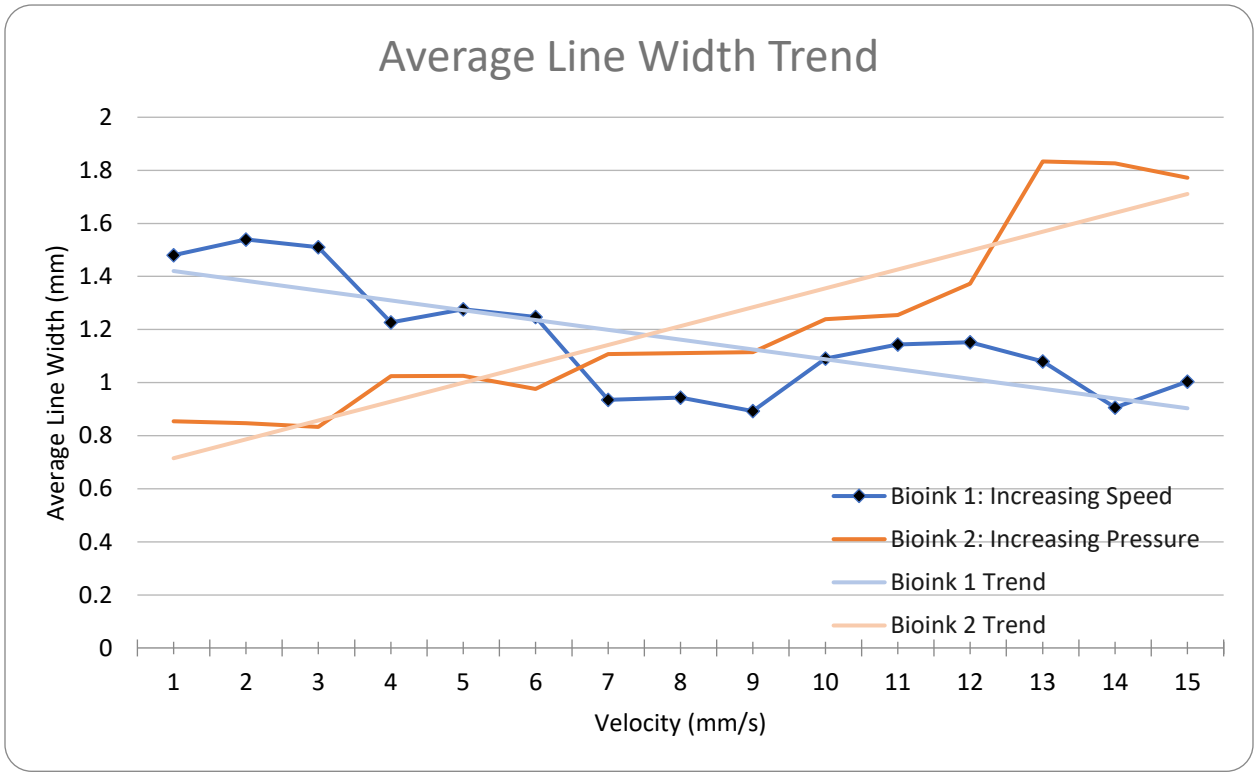

Figure 12: Average Line Width Trend Lines

Table 7: Bioink 1 Varying Speed Data (2% Gel ^% Alg)

Test	Line	Length	Area	Discontinuity	Line Width	Avg. Line Width
P=20, S=10	1.1	12.023	17.164		1.427597106	1.479760155
	1.2	14.486	21.788		1.504072898	
	1.3	13.534	20.404		1.507610463	
	2.1	12.704	18.912		1.488664987	1.539495325
	2.2	14.473	22.029		1.522075589	
	2.3	13.04	20.965		1.607745399	
	3.1	12.92	19.967		1.545433437	1.510860162
	3.2	14.488	20.981		1.448163998	
	3.3	11.8	18.16		1.538983051	
P=20, S=15	1.1	14.166	17.781		1.255188479	1.227076387
	1.2	14.286	17.449		1.221405572	
	1.3	14.196	17.101		1.204635108	
	2.1	14.289	17.759		1.242844146	1.27631665
	2.2	14.289	18.574		1.299881027	
	2.3	14.272	18.357		1.286224776	
	3.1	14.137	17.948		1.269576289	1.247204602
	3.2	14.287	18.053		1.263596276	
	3.3	14.287	17.265		1.20844124	
P=20, S=20	1.1	13.233	10.875		0.821809114	0.935059942
	1.2	14.464	11.674		0.807107301	
	1.3	12.209	14.361		1.176263412	
	2.1	14.26	12.015		0.84256662	0.943924384
	2.2	14.483	13.218		0.912656218	
	2.3	13.207	14.218		1.076550314	
	3.1	13.858	12.59		0.908500505	0.892652033
	3.2	14.523	12.6		0.867589341	
	3.3	12.86	11.598		0.901866252	
P=20, S=25	1.1	14.066	15.583		1.107848713	1.09105077
	1.2	14.394	15.65		1.08725858	
	1.3	14.261	15.374		1.078045018	
	2.1	14.371	16.583		1.153921091	1.143766168
	2.2	14.454	16.469		1.139407776	
	2.3	14.293	16.265		1.137969635	
	3.1	14.073	16.903		1.201094294	1.151584344
	3.2	14.456	16.205		1.120987825	
	3.3	14.291	16.187		1.132670912	
P=20, S=30	1.1	12.459	3.863+4.029	6.123	1.25	1.08
	1.2	10.09	9.392		0.930822597	
	1.3					
	2.1	11.365	9.878		0.869159701	0.905981106
	2.2	14.559	12.032		0.826430387	
	2.3	12.213	12.486		1.02235323	
	3.1	9.7	10.605		1.093298969	1.003251237
	3.2	14.529	13.178		0.907013559	
	3.3	11.757	11.868		1.009441184	

Descriptive Statistics

	N	Minimum	Maximum	Mean	
	Statistic	Statistic	Statistic	Statistic	Std. Error
Speed10	3	1.480	1.534	1.50833	.015645
Speed15	3	1.227	1.276	1.25000	.014224
Speed20	3	.893	.944	.92400	.015716
Speed25	3	1.091	1.152	1.12900	.019140
Speed30	3	.906	1.080	.99633	.050340
Valid N (listwise)	3				

Figure 13: Descriptive Statistics for varying speed

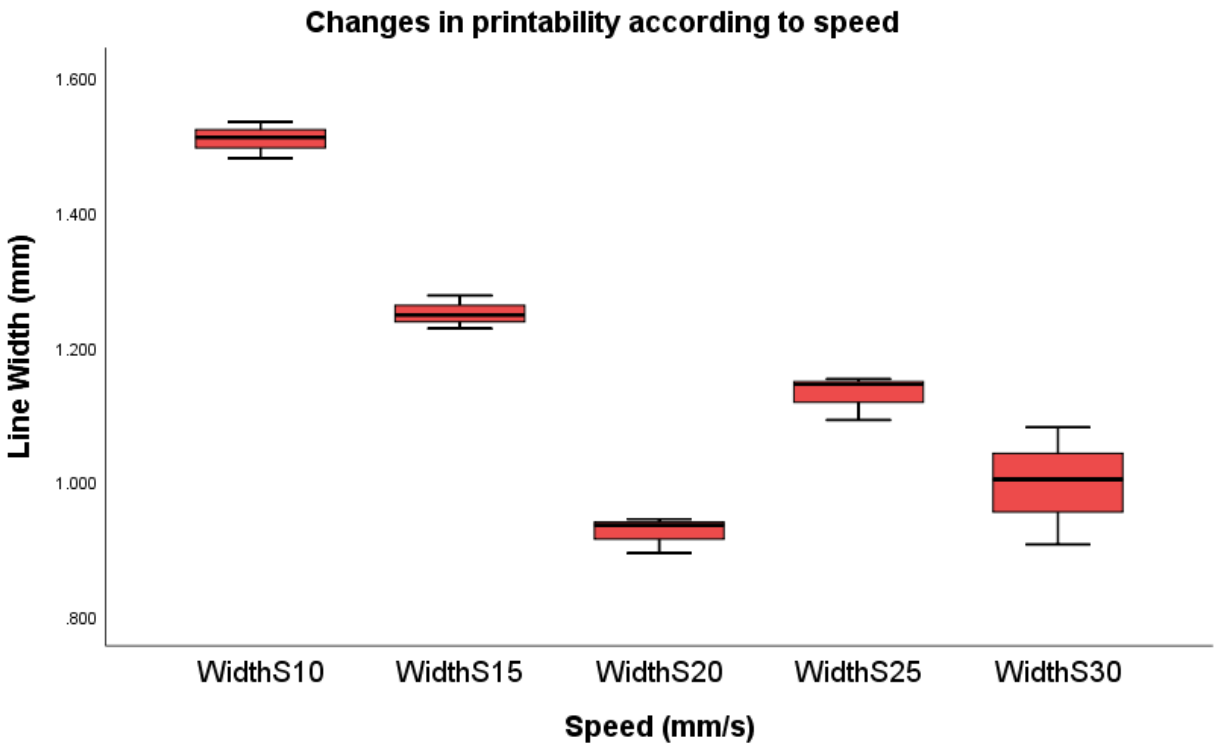

Figure 14: Boxplot for varying speed

Table 8: Bioink 2 Varying Pressure Data (2% Gel 6% Alg)

Test	Line	Length	Area	Mean	Line Width	Avg. Line Width

S=20, P=20	1.1	16.224	13.832	115.206	0.852564103	0.854088339
	1.2	16.641	13.822	112.827	0.830599123	
	1.3	16.121	14.172	109.886	0.879101793	
	2.1	16.276	12.858		0.789997542	0.847367019
	2.2	16.641	14.571		0.875608437	
	2.3	15.133	13.264		0.876495077	
	3.1	16.511	13.116		0.794379505	0.833079684
	3.2	16.615	14.388		0.86596449	
	3.3	15.313	12.846		0.838895056	
S=20, P=25	1.1	16.406	16.095		0.981043521	1.024389435
	1.2	16.616	16.885		1.016189215	
	1.3	16.514	17.768		1.07593557	
	2.1	16.459	15.643		0.950422261	1.025694383
	2.2	16.669	16.985		1.018957346	
	2.3	16.434	18.204		1.107703541	
	3.1	16.226	15.046		0.927277209	0.976596945
	3.2	16.59	16.196		0.976250753	
	3.3	16.411	16.842		1.026262872	
S=20, P=30	1.1	16.172	17.436		1.078159782	1.107032754
	1.2	16.641	17.854		1.072892254	
	1.3	16.225	18.984		1.170046225	
	2.1	16.328	17.014		1.042013719	1.111202759
	2.2	16.667	19.359		1.16151677	
	2.3	16.198	18.305		1.130077787	
	3.1	16.355	17.798		1.088229899	1.114310848
	3.2	16.667	18.116		1.086938261	
	3.3	16.094	18.794		1.167764384	
S=20, P=35	1.1	16.251	20.418		1.25641499	1.239139721
	1.2	16.642	21.367		1.283920202	
	1.3	16.303	19.19		1.177083972	
	2.1	16.354	22.222		1.3588113	1.254027038
	2.2	16.59	21.086		1.271006631	
	2.3	16.384	18.551		1.132263184	
	3.1	16.224	23.151		1.426960059	1.373394137
	3.2	16.667	23.385		1.403071939	
	3.3	16.488	21.272		1.290150412	
S=20, P=40	1.1	16.511	28.672		1.736539277	1.833395149
	1.2	16.641	31.176		1.873445105	
	1.3	16.512	31.211		1.890201066	
	2.1	16.355	29.24		1.787832467	1.826648246
	2.2	16.563	30.547		1.844291493	
	2.3	16.382	30.271		1.847820779	

3.1	16.432	28.642	1.743062317	1.771962841
3.2	16.667	29.472	1.768284634	
3.3	16.382	29.562	1.80454157	

Descriptive Statistics

	N	Minimum	Maximum	Mean	
	Statistic	Statistic	Statistic	Statistic	Std. Error
Pressure20	3	.833	.854	.84467	.006173
Pressure25	3	.977	1.026	1.00900	.016010
Pressure30	3	1.107	1.114	1.11067	.002028
Pressure35	3	1.239	1.373	1.28867	.042388
Pressure40	3	1.772	1.833	1.81067	.019411
Valid N (listwise)	3				

Figure 15:Descriptive statistics for changing pressure

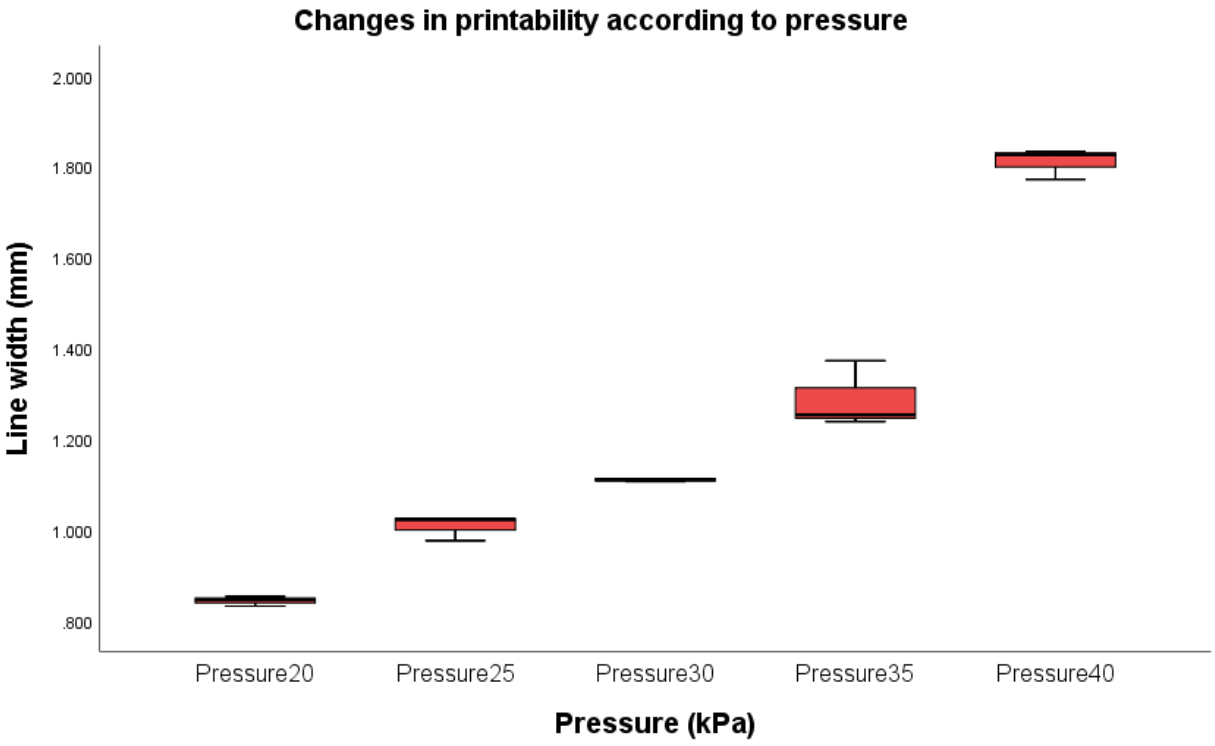

Figure 16: Boxplot for varying pressure

6. Conclusion

6.1. Closing Statements

3D bioprinting is an advancing technology that has emerged as a prime solution to address the challenges faced in tissue engineering. It became apparent that the printability of bioinks is the eminent challenge faced because it is the first step in the fabrication process. This thesis summarizes the research objectives and focus, being how manipulating 3D bioprinting parameters can ensure a consistent extrusion-based print by assessing the printability of bioinks. Printability is recognized as demonstrating smooth and continuous extrusions that accurately depict the CAD model of reference. Assessing the printability in new bioinks seems to be the first step in improving 3D bioprinting by defining a set of ideal printing parameters that contributed to optimal printability. It can be argued that the creation of a stable bioink concentration may as well be the first step. Both methods are addressed in this paper as having equal importance in contributing to the field of tissue engineering and additive manufacturing.

A crucial element that needs to be considered in the formulation of new bioinks include material selection. The importance of selecting hydrogel components depicts the possibility to extrude structures of good printability because of the bioink consistency criteria needing to be met prior to manipulating the printing parameters. Hydrogels with a gelatin base have been known for being attractive materials for biomedical applications. There are a wide range of gels with different mechanical properties and potential applications in different fields that can be produced through the correct control of the different experimental parameters [43] like the ones discussed in this thesis. The combination of GelMA and alginate emphasized the importance of understanding

hydrogel standards like temperature constraints that initiate the printing process. Heating the printhead to 37 degrees Celsius was an optimal parameter that consistently enabled depositing bioink. The information puts forth cogent data that was heavily reliant on analytical reasoning. Understanding the low viscous properties produced in the initial experiment could have shifted the entire experimental direction had the gelatin concentration been increased rather than the alginate. The research path taken could have also shifted routes dependent on the printing properties selected to remain variable. Amongst the many different printing properties, selecting print speed and pressure to be analyzed scientifically made sense because the pneumatic operation of the extrusion-based bioprinter application had the most effect on the bioink printability. Recalling the trend lines, it visibly is seen that adjusting printing speed and pressure, independently of one another each effect printability.

The gathered data in this thesis demonstrated that there exists a relationship between pressure and speed through the assessment of printability accuracy. This was concluded due to the near accuracy of the printed line width with respect to the dimensions of the CAD model which was prompted by the selection of hydrogels. One hundred percent printability accuracy would have been achieved for a structure with the same line width as the CAD model (0.2 mm). The best result obtained having the thinnest line width with mean 0.845 +/- 0.006 kPa remained within 62% accuracy. Through the assessment of printability, it can be assumed that the establishment of standard bioprinting parameters and bioink properties is needed for effectively making constructs with better shape fidelity.

6.2. Limitations and Future Work

There is still a great need of research to be done in this field before its applications are successfully implemented in the field of tissue engineering. Improving on the methodology of this thesis, CAD models like the one shown in Figure 17 are proposed for future research in bioprinting because it expands on the assessment of printability by further analyzing the effects of the structure along the Z axis. Image a, b, and c are testing the connecting node to observe any improper layovers that occur when merging to analyze key methods for printing layered structures in 3D. Moving forward from testing how layers adhere to each other, Figure 18 advances the CAD model to a matrix that tests for filament collapse at ten layers to assess the printability of the bioink for structural integrity to define other factors that contribute reasonable printability.

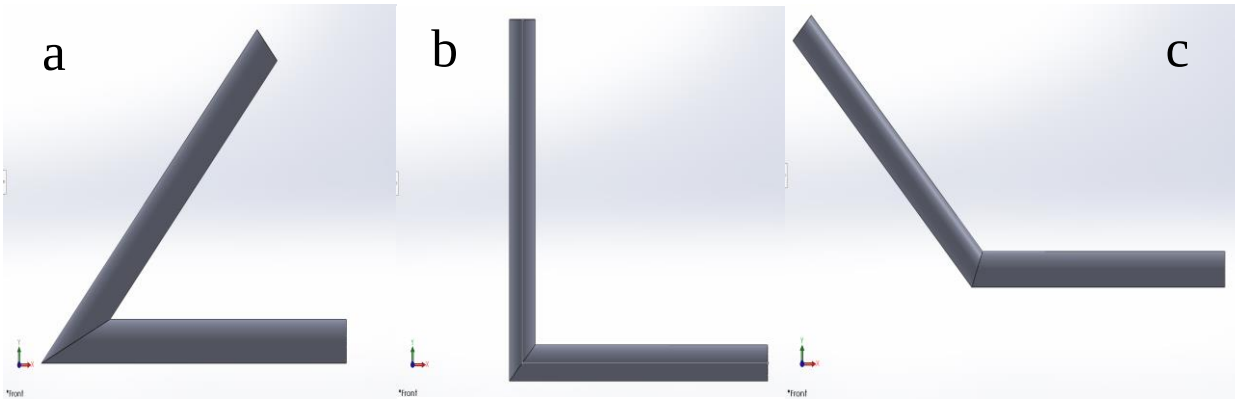

Figure 17: 3D CAD (a) Acute Angle (45°), (b) Right Angle (90°), (c) Obtuse Angle (135°)

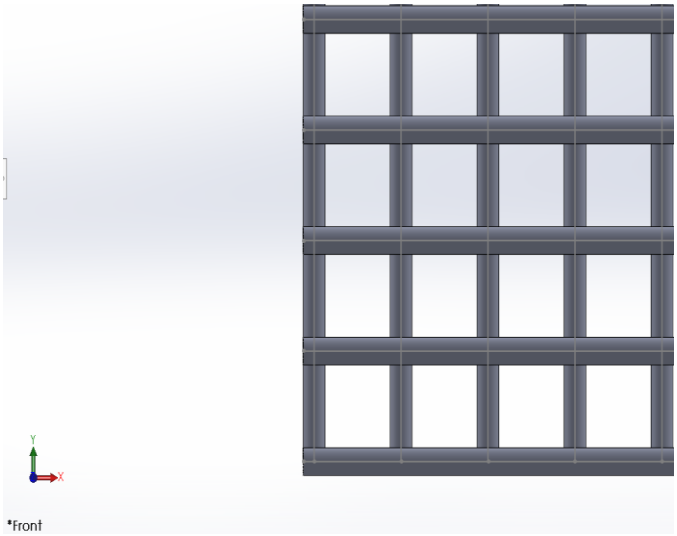

Figure 18: 10-layer CAD model scaffold

Amongst many other researchers, the author embarked on an endeavor to contribute to the advancement of 3D bioprinting technology. There are several features in this study that can be amended for future work.

For instance, the most apparent attempt to meliorate this study would be to include the photo initiator to apply these methods in actual tissue engineering applications. Biofabricated organs will cease to exist without photo initiators which are in conjunction with cell viability. Photo initiators need to be cross-linked which enable features such as cell migration, nutrients and oxygen diffusion, and new tissue formation [45]. There are different types of cross-linking methods and they will vary depending on the material and type of cell chosen. Cross-linking should be used in future works to retain shape fidelity by rapid curing methods and improving on the printed elasticity. This would require the calculation of the shear modulus for experimental results. Study duration is a key element that plays a factor in determining what feasible accomplishments research can achieve. This study was conducted over the course of two semesters (approximately 9 months) and was limited by external circumstances that unfortunately reduced the capability of

physical lab appearance. This paper should be used as a reference for more tests to be conducted and improved upon. With more time, cell selection would have occurred to begin the cross-linking process. A longer study would also route for different test parameters to be considered when monitoring the mechanical behavior.

Moreover, in alignment with the two test parameters selected in this study (speed and pressure) a sub experiment could be performed to test to what extent the pressure and speed can reach while maintaining a structured print. It was concluded that the optimal parameters for the corresponding bioink concentration was found at a pressure of 20 kPa and a speed of 20 mm/s. These values correlate to the series of five experiments performed per concentration but are not limited by these values. In fact, future studies should exceed this pressure baseline and adjust the corresponding speed to establish the maximum pressure that can be achieved without hindering the printability. Once these parameters have distinguished maximum and minimum values, other parameters should then be explored to further improve the structure.

Furthermore, as previously mentioned in this paper ImageJ, although useful did not provide accurate result depiction as seen in *Figure 22: 8-bit image rendering* provides a visual at the noise captured in the image. A future researcher should either a) become more familiar with the software because there may be feature add-ins such as edge detection that could disregard the noise and solely focus on capturing the desired image or b) educate themselves with a more appropriate software that can just as easily, but more accurately compile data. It was apparent in the early stages that ImageJ was not easily compatible with the initial extruded bioink concentration that did not contain food coloring because its transparency did not allow for the automatic image processing. This prompted the purchase and inclusion of the food coloring. Based on these

experimental observations and data analyses, the previous statements in this section are only the author recommendations to further advance the research being conducted in 3D bioprinting in order to assess printability while simultaneously building upon this documented research.

Appendix A: ImageJ Data

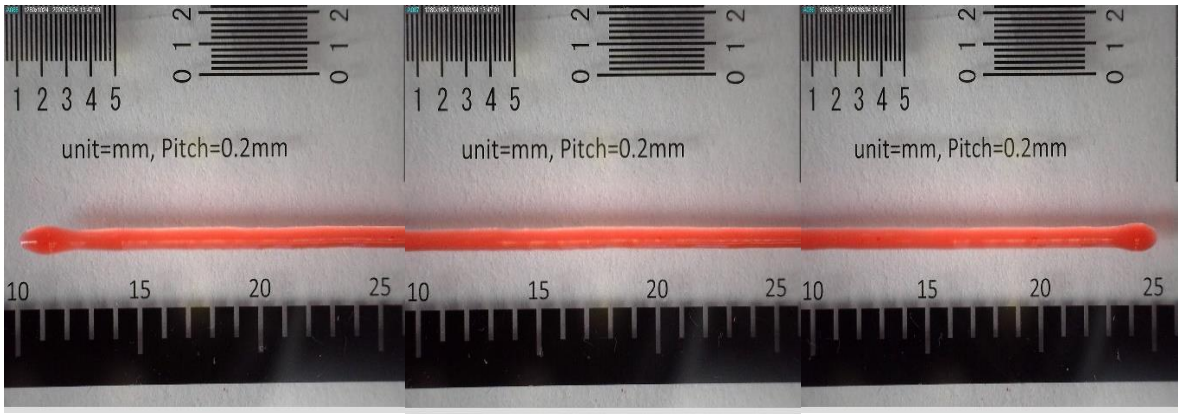

Figure 19: Dino captured image of extruded bioink at low pressure and high speed

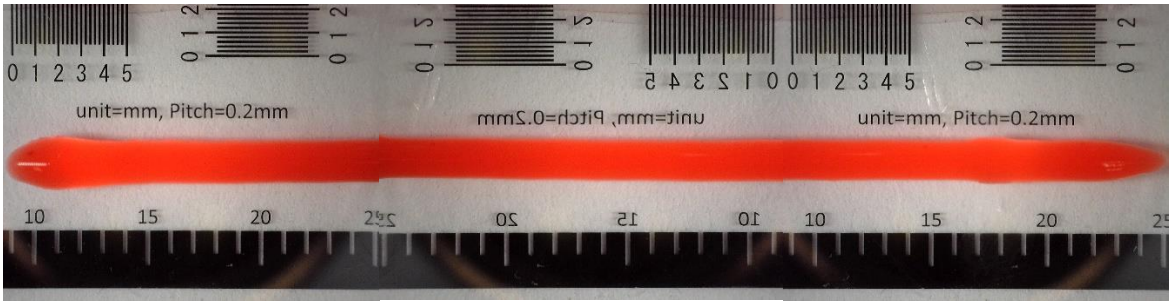

Figure 20: Dino captured image of extruded bioink at high pressure and low speed

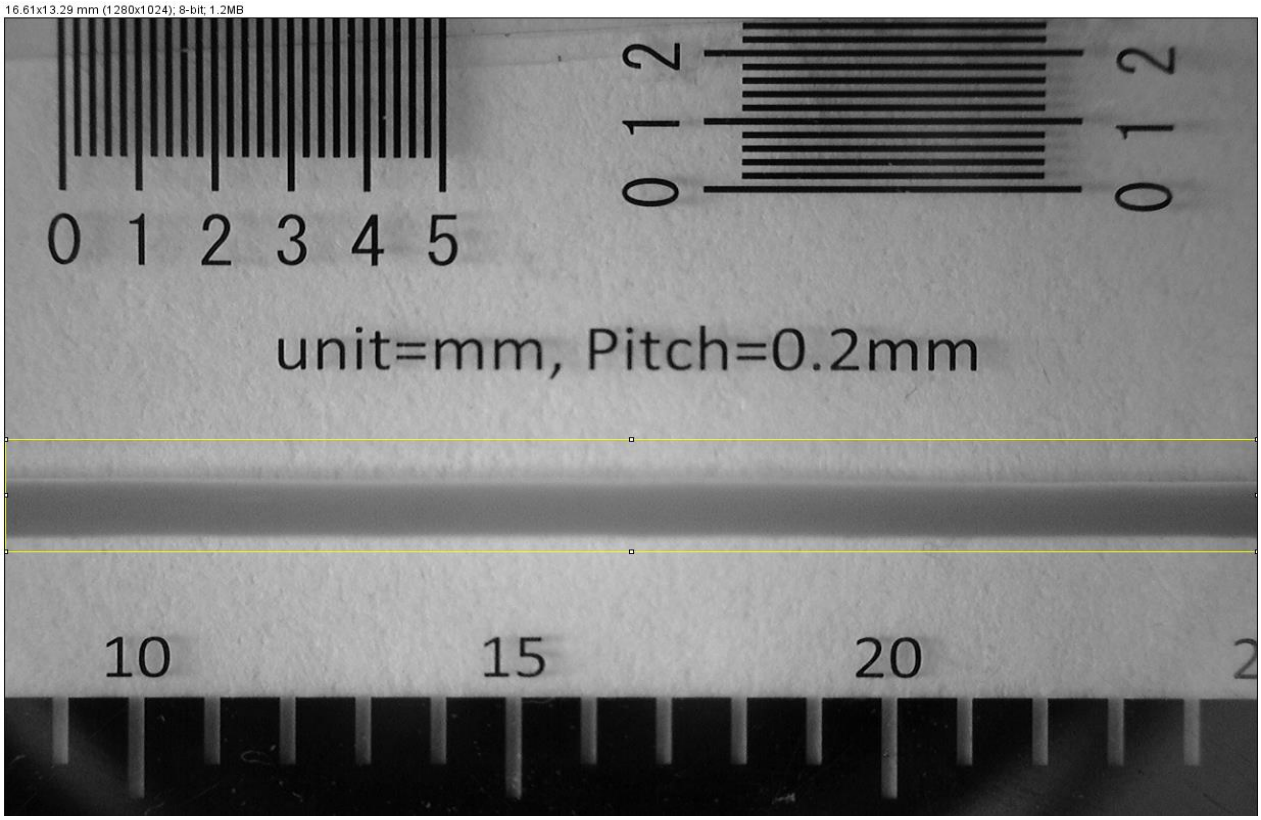

Figure 21: Distinguished target area to be captured

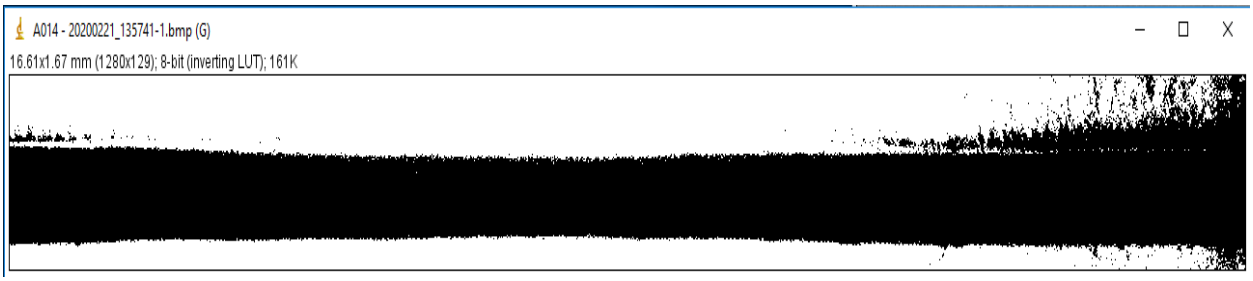

Figure 22: 8-bit image rendering

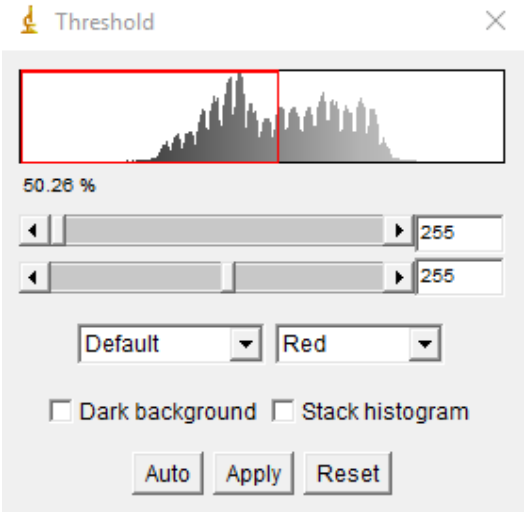

Figure 23: Threshold adjustment

Appendix B: Excel Results

Table 9: Results of bioink properties, printed at a pressure of 20kPa and a speed of 20 mm/s

	Area	Mean	Min	Max
1	0.003	255	255	255
2	0.002	255	255	255
3	0.004	255	255	255
4	0.001	255	255	255
5	0.009	255	255	255
6	1.68E-04	255	255	255
7	1.68E-04	255	255	255
8	5.05E-04	255	255	255
9	0.001	255	255	255
10	1.68E-04	255	255	255
11	1.68E-04	255	255	255
12	1.68E-04	255	255	255
13	0.002	255	255	255
14	0.006	255	255	255
15	12.001	255	255	255
16	1.68E-04	255	255	255
17	8.42E-04	255	255	255
18	1.68E-04	255	255	255
19	1.68E-04	255	255	255
20	1.68E-04	255	255	255
21	5.05E-04	255	255	255
22	1.68E-04	255	255	255
23	1.68E-04	255	255	255
24	1.68E-04	255	255	255
25	1.68E-04	255	255	255
26	1.68E-04	255	255	255
27	1.68E-04	255	255	255
28	1.68E-04	255	255	255
29	0.001	255	255	255
30	0.003	255	255	255
31	1.68E-04	255	255	255
32	5.05E-04	255	255	255

Table 10: Results of bioink properties, printed at a pressure of 25 kPa and a speed of 20 mm/s

	Area	Mean	Min	Max
1	0.003	255	255	255
2	0.015	255	255	255
3	5.05E-04	255	255	255
4	0.001	255	255	255
5	3.37E-04	255	255	255
6	1.68E-04	255	255	255
7	1.68E-04	255	255	255
8	1.68E-04	255	255	255
9	5.05E-04	255	255	255
10	1.68E-04	255	255	255
11	3.37E-04	255	255	255
12	1.68E-04	255	255	255
13	0.002	255	255	255
14	1.68E-04	255	255	255
15	5.05E-04	255	255	255
16	3.37E-04	255	255	255
17	0.001	255	255	255
18	1.68E-04	255	255	255
19	11.233	255	255	255
20	1.68E-04	255	255	255
21	1.68E-04	255	255	255
22	3.37E-04	255	255	255
23	1.68E-04	255	255	255
24	3.37E-04	255	255	255
25	1.68E-04	255	255	255
26	1.68E-04	255	255	255
27	6.74E-04	255	255	255
28	6.74E-04	255	255	255
29	1.68E-04	255	255	255
30	5.05E-04	255	255	255
31	1.68E-04	255	255	255
32	3.37E-04	255	255	255

Table 11: Results of bioink properties, printed at a pressure of 30 kPa and a speed of 20 mm/s

	Area	Mean	Min	Max
1	5.05E-04	255	255	255
2	0.003	255	255	255
3	1.68E-04	255	255	255
4	11.169	255	255	255
5	1.68E-04	255	255	255
6	1.68E-04	255	255	255
7	1.68E-04	255	255	255
8	8.42E-04	255	255	255
9	1.68E-04	255	255	255
10	1.68E-04	255	255	255
11	6.74E-04	255	255	255
12	1.68E-04	255	255	255
13	0.004	255	255	255
14	0.003	255	255	255
15	0.003	255	255	255
16	3.37E-04	255	255	255
17	3.37E-04	255	255	255
18	8.42E-04	255	255	255
19	8.42E-04	255	255	255
20	0.006	255	255	255
21	1.68E-04	255	255	255
22	1.68E-04	255	255	255
23	6.74E-04	255	255	255
24	0.01	255	255	255
25	1.68E-04	255	255	255
26	1.68E-04	255	255	255
27	6.74E-04	255	255	255
28	1.68E-04	255	255	255
29	5.05E-04	255	255	255
30	1.68E-04	255	255	255
31	1.68E-04	255	255	255
32	1.68E-04	255	255	255

Table 12: Results of bioink properties, printed at a pressure of 35 kPa and a speed of 20 mm/s

	Area	Mean	Min	Max
1	5.05E-04	255	255	255
2	1.68E-04	255	255	255
3	5.05E-04	255	255	255
4	1.68E-04	255	255	255
5	3.37E-04	255	255	255
6	5.05E-04	255	255	255
7	0.006	255	255	255
8	1.68E-04	255	255	255
9	5.05E-04	255	255	255
10	3.37E-04	255	255	255
11	6.74E-04	255	255	255
12	1.68E-04	255	255	255
13	0.001	255	255	255
14	13.229	255	255	255
15	1.68E-04	255	255	255
16	3.37E-04	255	255	255
17	1.68E-04	255	255	255
18	1.68E-04	255	255	255
19	0.007	255	255	255
20	1.68E-04	255	255	255
21	3.37E-04	255	255	255
22	8.42E-04	255	255	255
23	1.68E-04	255	255	255
24	3.37E-04	255	255	255
25	1.68E-04	255	255	255
26	3.37E-04	255	255	255
27	5.05E-04	255	255	255
28	3.37E-04	255	255	255
29	3.37E-04	255	255	255
30	1.68E-04	255	255	255
31	1.68E-04	255	255	255
32	1.68E-04	255	255	255

Table 13: Results of bioink properties, printed at a pressure of 40 kPa and a speed of 20 mm/s

	Area	Mean	Min	Max
1	1.68E-04	255	255	255
2	0.002	255	255	255
3	1.68E-04	255	255	255
4	3.37E-04	255	255	255
5	13.334	255	255	255
6	1.68E-04	255	255	255
7	1.68E-04	255	255	255
8	1.68E-04	255	255	255
9	8.42E-04	255	255	255
10	1.68E-04	255	255	255
11	1.68E-04	255	255	255
12	1.68E-04	255	255	255
13	1.68E-04	255	255	255
14	0.001	255	255	255
15	0.001	255	255	255
16	3.37E-04	255	255	255
17	1.68E-04	255	255	255
18	1.68E-04	255	255	255
19	1.68E-04	255	255	255
20	1.68E-04	255	255	255
21	1.68E-04	255	255	255
22	1.68E-04	255	255	255
23	1.68E-04	255	255	255
24	1.68E-04	255	255	255
25	3.37E-04	255	255	255
26	8.42E-04	255	255	255
27	1.68E-04	255	255	255
28	0.001	255	255	255
29	3.37E-04	255	255	255
30	3.37E-04	255	255	255
31	1.68E-04	255	255	255
32	1.68E-04	255	255	255

References

[1] Mironov, V.; Boland, T.; Trusk, T.; Forgacs, G.; Markwald, R.R. Organ printing: Computer-aided jet-based 3D tissue engineering. Trends Biotechnol. 2003, 21, 157–161

[2] Derby, B. Printing and prototyping of tissues and scaffolds. Science 2012, 338, 921–926

[3] Naomi Paxton et al 2017 Biofabrication 9 044107

[4] Jungst, T.; Smolan, W.; Schacht, K.; Scheibel, T.; Groll, J.r. Strategies and molecular design criteria for 3D printable hydrogels. Chem. Rev. 2016, 116, 1496–1539

[5] Nakamura, M.; Nishiyama, Y.; Henmi, C.; Yamaguchi, K.; Mochizuki, S.; Koki, T.; Nakagawa, H. Inkjet Bioprinting as an Effective Tool for Tissue Fabrication. In Proceedings of the NIP & Digital Fabrication Conference, Denver, CO, USA, 17–22 September 2006

[6] Suárez-González, D.; Barnhart, K.; Migneco, F.; Flanagan, C.; Hollister, S.J.; Murphy, W.L. Controllable mineral coatings on PCL scaffolds as carriers for growth factor release. Biomaterials 2012, 33, 713–721

[7] Sánchez-Salcedo,S.;Colilla,M.;Izquierdo-Barba,I.;Vallet-Regí,M.Preventingbacterialadhesiononscaffolds for bone tissue engineering. Int. J. Bioprinting 2016, 2, 20–34

[8] Axpe, E., & Oyen, M. (2016). Applications of Alginate-Based Bioinks in 3D Bioprinting. International Journal of Molecular Sciences, 17(12), 1976. MDPI AG. Retrieved from http://dx.doi.org/10.3390/ijms17121976

[9] Applied Physics Reviews 5, 041112 (2018)

[10] T. Jiang, J. G. Munguia-Lopez, S. Flores-Torres, J. Grant, S. Vijayakumar, A. Leon-Rodriguez, and J. M. Kinsella, Sci. Rep. 7(1), 4575 (2017)

[11] M. E. Pepper, V. Seshadri, T. Burg, B. W. Booth, K. J. L. Burg, and R. E. Groff, paper presented at the 2011 Annual International Conference of the IEEE Engineering in Medicine and Biology Society, 2011

[12] M. E. Pepper, V. Seshadri, T. C. Burg, K. J. Burg, and R. E. Groff, Biofabrication 4(1), 011001 (2012)

[13] M. Nakamura, S. Iwanaga, C. Henmi, K. Arai, and Y. Nishiyama, Biofabrication 2(1), 014110 (2010)

[14] B. Hopp, T. Smausz, N. Kresz, N. Barna, Z. Bor, L. Kolozsvari, D. B. Chrisey, A. Szabo, and A. Nogradi, Tissue Eng. 11(11–12), 1817–1823 (2005)

[15] L. Koch, S. Kuhn, H. Sorg, M. Gruene, S. Schlie, R. Gaebel, B. Polchow, K. Reimers, S. Stoelting, N. Ma, P. M. Vogt, G. Steinhoff, and B. Chichkov, Tissue Eng., Part C 16(5), 847–854 (2010)

[16] B. Guillotin, A. Souquet, S. Catros, M. Duocastella, B. Pippenger, S. Bellance, R. Bareille, M. Remy, L. Bordenave, J. Amedee, and F. Guillemot, Biomaterials 31(28), 7250–7256 (2010)

[17] S. V. Murphy and A. Atala, Nat. Biotechnol. 32(8), 773–785 (2014)

[18] B. Guillotin and F. Guillemot, Trends Biotechnol. 29(4), 183–190 (2011)

[19] B. Guillotin, A. Souquet, S. Catros, M. Duocastella, B. Pippenger, S. Bellance, R. Bareille, M. Remy, L. Bordenave, J. Amedee, and F. Guillemot, Biomaterials 31(28), 7250–7256 (2010).

[20] V. Mironov, R. P. Visconti, V. Kasyanov, G. Forgacs, C. J. Drake, and R. R. Markwald, Biomaterials 30(12), 2164–2174 (2009)

[21] K. Nair, M. Gandhi, S. Khalil, K. C. Yan, M. Marcolongo, K. Barbee, and W. Sun, Biotechnol. J. 4(8), 1168–1177 (2009)

[22] A. Blaeser, D. F. Duarte Campos, U. Puster, W. Richtering, M. M. Stevens, and H. Fischer, Adv. Healthcare Mater. 5(3), 326–333 (2016)

[23] R. Chang, J. Nam, and W. Sun, Tissue Eng., Part A 14(1), 41–48 (2008)

[24] Vijayavenkataraman, Sanjairaj, W. F. Lu, and J. Y. H. Fuh. "3D bioprinting of skin: a state-of-the-art review on modelling, materials, and processes." Biofabrication 8.3 (2016): 032001

[25] Nair, K.; Gandhi, M.; Khalil, S.; Yan, K.C.; Marcolongo, M.; Barbee, K.; Sun, W. Characterization of cell viability during bioprinting processes. Biotechnol. J. 2009, 4, 1168–1177

[26] Panwar, A., & Tan, L. (2016). Current Status of Bioinks for Micro-Extrusion-Based 3D Bioprinting. Molecules, 21(6), 685. MDPI AG. Retrieved from http://dx.doi.org/10.3390/molecules21060685

[27] D. Beski, T. Dufour, F. Gelaude, A. Ilankovan, M. Kvasnytsia, M. Lawrenchuk, I. Lukyanenko, M. Mir, L. Neumann, A. Nguyen, A. Soares, E. Sauvage, K. Vanderperren, and D. Vangeneugden, “Software for biofabrication,” in Essentials of 3D Biofabrication and Translation, edited by A. Atala and J. J. Yoo (Academic Press, Boston, 2015), Chap. 2, pp. 19–41

[28] S. Junk and C. Kuen, “Review of open source and freeware CAD systems for use with 3D-printing,” Procedia CIRP 50, 430–435 (2016)

[29] He, Y. et al. Research on the printability of hydrogels in 3D bioprinting. Sci. Rep. 6, 29977; doi: 10.1038/srep29977 (2016)

[30] Bertassoni, L. E. et al. Direct-write bioprinting of cell-laden methacrylated gelatin hydrogels. Biofabrication. 6, 024105 (2014)

[31] Liliang Ouyang *et al* 2016 *Biofabrication* **8** 035020

[32] Ouyang L, Yao R, Chen X, Na J and Sun W 20153D printing of HEK293FT cell-laden hydrogel into microporous constructs with high cell viability and normal biological functions Biofabrication7015010

[33] ZhaoYetal 2014 Three-dimensional printing of Helacells for cervical tumor model in vitro Biofabrication 6035001

[34] Rutz A L, Hyland K E, Jakus A E, Burghardt W Rand Shah R N 2015 A multi material bioink method for 3D printing tunable, cell-compatible hydrogels Adv. Mater. 271607–14

[35] SkardalAetal2015Ahydrogelbioinktoolkitformimicking native tissue biochemical and mechanical properties in bioprinted tissue constructs Act a Biomater. 2524–34

[36] Tabriz A G, Hermida M A, Leslie N Rand Shu W 2015 Three dimensional bioprinting of complex cell laden alginate hydrogel structures Biofabrication 7045012

[37] Hockaday L A et al 2012 Rapid 3D printing of anatomically accurate and mechanically heterogeneous aortic valve hydrogel scaffolds Biofabrication 4035005

[38] Jakus A E, Rutz A L and Shah R N 2016 Advancing the field of 3D biomaterial printing Biomed. Mater. 11014102

[39] Yurtoğlu, N. (2018). Research on the printability of hydrogels in 3D bioprinting. History Studies International Journal of History, 10(7), 241–264. doi: 10.9737/hist.2018.658

[40] A Ribeiro et al 2018 Biofabrication 10 014102

[41] BIO X™ - The go-to bioprinter for life-science companies, researchers and innovators. (n.d.). Retrieved from https://cellink.com/bioprinting/bio-x/

[42] M. Djabourov, J.P. Lechaire, F. Gaill Structure and rheology of gelatin and collagen gels

Biorheology, 30 (3–4) (1993), pp. 191-205

[43] Van Den Bulcke AI, Bogdanov B, De Rooze N, Schacht EH, Cornelissen M, Berghmans H. Structural and rheological properties of methacrylamide modified gelatin hydrogels. Biomacromolecules, 2000, 1: 31–38

[44] Naomi Paxton et al 2017 Biofabrication 9 044107

[45] Aljohani, W., Ullah, M. W., Zhang, X., & Yang, G. (2017, September 21). Bioprinting and its applications in tissue engineering and regenerative medicine. Retrieved from https://www.sciencedirect.com/science/article/pii/S0141813017325862?via=ihub